Supplementary information for: "Quantum Bi-stability and Robust Room-Temperature Spin Excitation in a Single-Ion Magnet"

Gourab Roy, Mohit Kumar, Jhuma Sannigrahi, Vincent Caignaert, Devashibhai T. Adroja, Ekta Kushwaha, Sayan Ghosh, Wilfrid Prellier, Vincent Hardy, and Tathamay Basu*

E-mail: tathamay.basu@rgipt.ac.in

Contents of the Supplementary information

Analysis of Neutron Diffraction (ND)

Neutron diffraction measurements were performed on a polycrystalline sample of $Sr_2Ca_2Mn_2CoO_9$ using the HRPT diffractometer at PSI, covering a wide Q range from 0.27 to 8.3 $Å^{-1}$ (corresponding to 3.75° to 164.7° in 2θ), with a neutron wavelength of 1.494 Å, at temperatures of 300 K and 5 K. The Rietveld refinements are shown in Figures S1a and S1b, respectively. The high-quality refinements confirm that the sample crystallises in the desired space group,

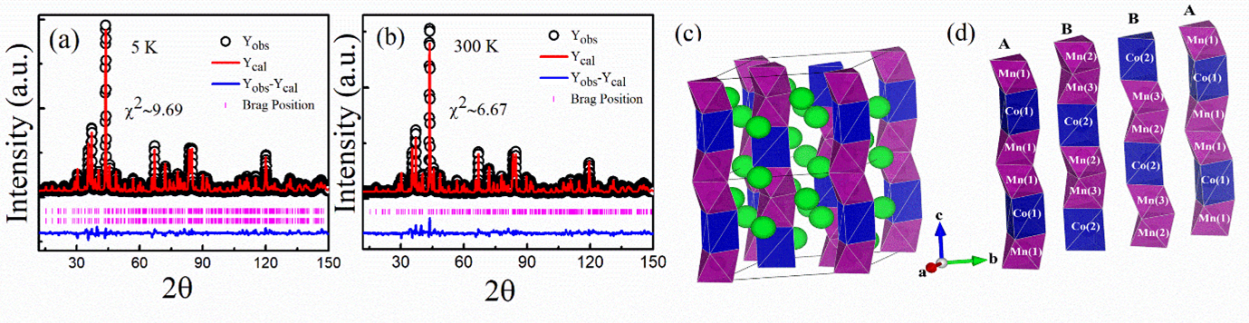

Figure 1: (a) Rietveld refinement of the neutron powder diffraction data at 5 K and (b) 300 K with PSI (HRPT) data. The Rietveld fitting is shown by the red solid line, while the experimental data are represented by open black circles. The vertical bars indicate the positions of Bragg peaks corresponding to the crystal and magnetic structures, respectively. The continuous blue line at the bottom shows the difference between the observed and calculated intensities. (c) Crystal structure of $Sr_2Ca_2Mn_2CoO_9$ at 5 K. The spin chains consist of MnO_6 (violet polyhedra) and CoO_6 (blue polyhedra), with Ca (red spheres) and Sr (green spheres) located between the spin chains. (d) Illustration of three spin chains connected body-diagonally within the unit cell.

and no structural change is observed upon cooling, retaining the trigonal $P321$ nuclear cell. The crystal structures obtained from the refinements are shown in Figures S1c and S1d for 300 K and 5 K, respectively. The cell parameters, atomic positions, thermal parameters, and occupancies of the nuclear structure obtained from the Rietveld refinement are listed in TABLE ST1 for 5 K and 300 K. Additional weak reflections appear at $Q = 1.08$, 1.67, and 2.1 Å^{-1} (corresponding to 15°, 23.7°, and 30.1° in 2θ) in the 5 K diffraction pattern, compared to that at 300 K, indicating the onset of magnetic ordering. To examine the nature of these additional Bragg peaks, temperature-dependent neutron diffraction measurements were carried out down to 5 K using the G4.1 diffractometer (wavelength 2.425 Å) at LLB, France. The LLB data, collected over a shorter Q range, contain fewer crystallographic Bragg peaks. Therefore, the structural refinement parameters were fixed based on the HRPT (PSI) data, which were obtained from a broader Q range and yielded reliable crystallographic fits. The Rietveld refinement of the LLB data at 300 K is shown in Figure S2d, while the magnetic refinements performed at various temperatures are displayed in Figures S2b–S2c.

Analysis of the diffraction data reveals the presence of magnetic long-range order (LRO),

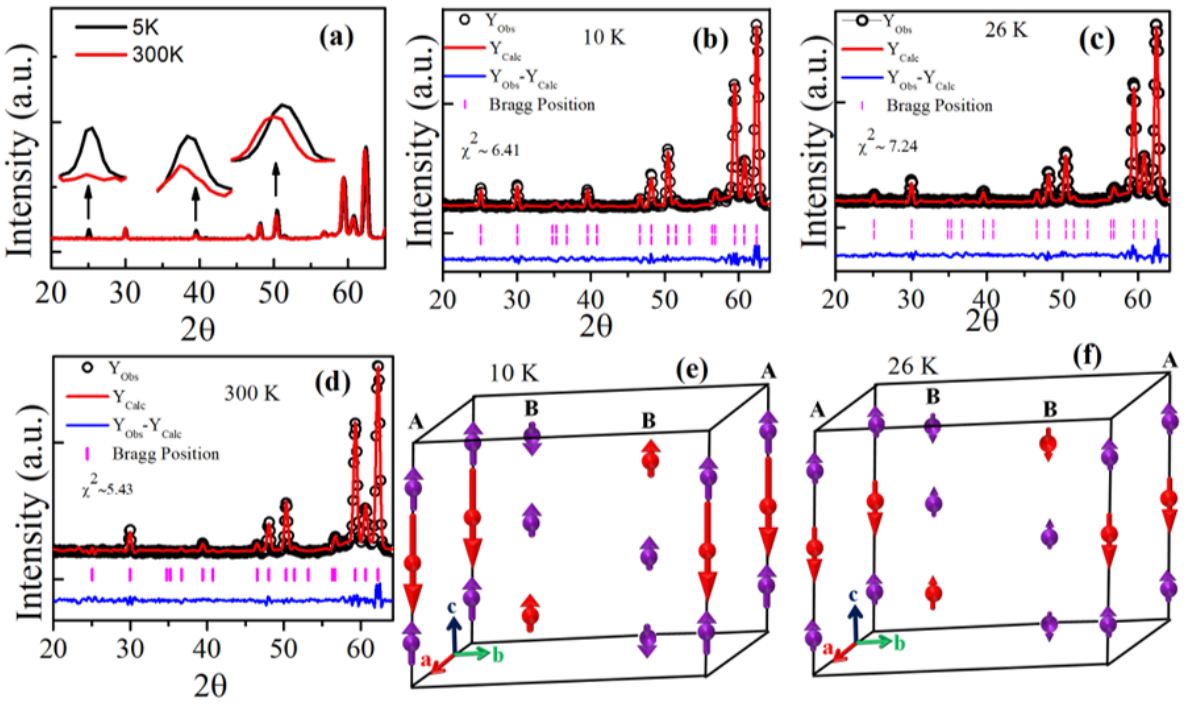

Figure 2: (a) Temperature comparison of the neutron powder diffraction (NPD) peak at room temperature (300 K) and below the magnetic ordering temperature. (b–d) Rietveld refinement of the NPD patterns collected at (b) 5 K, (c) 26 K, and (d) 300 K. The red solid line represents the calculated Rietveld fit, while the open black circles denote the experimental data. Vertical tick marks indicate the Bragg peak positions corresponding to the crystal and magnetic structures, respectively. The continuous blue line at the bottom shows the difference between the observed and calculated intensities. (e) Magnetic structure at 10 K and (f) 26 K.

indicated by the emergence of three magnetic Bragg peaks below the ordering temperature. These peaks are observed at $(1, 0, 1)/(0, 1, 1)$, $(2, 0, 1)/(0, 2, 1)$, and $(2, 1, 1)/(1, 2, 1)$. Among them, the $(1, 0, 1)/(0, 1, 1)$ peak, located at 25.10°, is the most prominent, showing a significant increase in intensity with decreasing temperature (see Fig. S2(a)). Since there are five magnetic sites in the unit cell, this assumption introduces five variables, resulting in multiple possible configurations. The magnetic peaks observed in this system are very small compared to the other crystal peaks.

The magnetic representation of a crystallographic site can then be decomposed in terms of the irreducible representations (IRs) as

$$\Gamma_{\mathrm{mag}} = \sum_{\nu} n_{\nu} \Gamma_{\nu}^{\mu},$$

where n_ν is the number of times that the IR Γ_ν^μ of order μ appears in the magnetic representation Γ_{mag} for the chosen crystallographic site. The decomposition of the magnetic representation of Mn(1), Mn(2), Mn(3), and Co(2) for $\mathbf{K} = (0, 0, 0)$ are given by

$$\Gamma_{\mathrm{mag}} = 1\Gamma_1^1 + 1\Gamma_2^1 + 2\Gamma_3^2$$

and

$$0\Gamma_1^1 + 1\Gamma_2^1 + 2\Gamma_3^2,$$

respectively, whereas for Co(1) it is

$$0\Gamma_1^1 + 1\Gamma_2^1 + 1\Gamma_3^2.$$

The corresponding possible basis vectors for the five magnetic atoms are provided in Table ST2 for Mn(1), Mn(2), Mn(3), and Co(2), and in Table ST3 for Co(1).

In neutron diffraction, only the component of the magnetic moment perpendicular to the scattering vector $\mathbf{Q}$ contributes to the magnetic intensity. However, for the $(1, 0, 1)/(0, 1, 1)$ reflections, pseudo-symmetry makes it difficult to determine the exact moment direction from the Bragg peak intensities. A similar limitation applies to the second magnetic peak at $(2, 0, 1)/(0, 2, 1)$. By contrast, the third magnetic peak at $(2, 1, 1)/(1, 2, 1)$ does not show a strong enhancement and remains relatively weak in magnetic intensity, making it equally challenging to deduce the moment orientation from this reflection alone. Tables ST1 and ST2 list all possible basis vectors corresponding to each magnetic atom. To further investigate the moment orientation, we examined the magnetic space group corresponding to the parent space group $P321$ (No. 150). Two magnetic subgroups are possible, namely $P321$ (150.25) and $P3_2'1$ (150.27). The allowed moment directions for each Wyckoff position are summarized

in Table ST4. The relevant Wyckoff positions of the magnetic atoms are Mn(1) at $(0, 0, z)$, Co(1) at $(0, 0, 1/2)$, and Mn(2), Mn(3), and Co(2) at $(1/3, 2/3, z)$, with their corresponding magnetic moment directions shown. From Table ST4, it is evident that the magnetic atoms in this structure are expected to align along the c-axis with such Wyckoff positions. However, in the magnetic space group $P321$ (150.25), Co(1) at $(0, 0, z)$ carries no moment, whereas in $P3_2'1$ (150.27), the same position supports a nonzero moment along the c direction. This indicates that the magnetic moments in this system are consistent with the $P3_2'1$ (150.27) magnetic space group. According to Table ST4 for $P3_2'1$ (150.27), the magnetic atoms align strictly along the c-axis, with symmetry-related equivalent sites such as $(1/3, 2/3, z)$ and $(2/3, 1/3, -z)$, or $(0, 0, z)$ and $(0, 0, -z)$, coupled through ferromagnetic interactions. Therefore, the correct magnetic space group for this system is $P3_2'1$ (150.27), where all moments are constrained along the c-axis and interact ferromagnetically at their equivalent symmetry-related positions.

Based on the magnetic space group understanding, we found that the best refinement results were obtained with the $\Gamma_2(\Psi_2)$ representation for Mn(1), Mn(2), Mn(3), and Co(2), and $\Gamma_2(\Psi_1)$ for Co(1). The Mn(1), Mn(2), Mn(3), and Co(2) atoms, which occupy identical crystallographic sites at Wyckoff positions (x, y, z) and $(x, y, -z)$, exhibit ferromagnetic interactions along the c-axis. In contrast, Co(1) occupies a single crystallographic site with $(0, 0, 0.5)$ along the c-axis. Table ST5 presents the irreducible representations and basis vectors for the two Co sites and three Mn sites in the $P321$ space group, with a propagation vector $\mathbf{k} = (0, 0, 0)$. A similar alignment of Ising spins along the c-axis has been reported previously in this system (see Ref. 16 in the main text). The magnetic structure was refined using the FullProf suite and the SARAh program.[1,2] After crystal and magnetic refinement, the metal–metal (M–M) or metal–oxygen (M–O) bond lengths and metal–oxygen–metal (M–O–M) bond angles were calculated using the VESTA software.[3]

Initially, we adjusted both Co^{2+} moments to match the magnetic peak in the neutron diffraction (ND) pattern. At a temperature of 5 K, the magnetic moment of Co(1) was

Table 1: Atomic coordinates of $Sr_2Ca_2Mn_2CoO_9$ (space group P321) at 5 K and 300 K, with estimated errors.

5 K ($a = b = 9.3652(2)$ Å, $c = 7.6945(3)$ Å, $\alpha = \beta = 90°$, $\gamma = 120°$)					
Atom (Site)	x	y	z	B_{iso}	Occupancy
Mn1	0.0000	0.0000	0.1740(4)	0.6823(4)	0.3245(6)
Mn2	0.3333	0.6667	0.0710(2)	0.6823(4)	0.3157(7)
Mn3	0.3333	0.6667	0.3947(2)	0.6823(3)	0.3144(5)
Co1	0.0000	0.0000	0.5000	0.6823(5)	0.1667(3)
Co2	0.3333	0.6667	0.7755(3)	0.6823(4)	0.3333(1)
Sr1	0.0209(2)	0.6878(4)	0.2478(3)	0.5807(3)	0.3700(1)
Ca1	0.0209(2)	0.6878(3)	0.2478(2)	0.5807(3)	0.6300(1)
Sr2	0.3464(2)	0.0000	0.5000	0.5807(3)	0.3500(5)
Ca2	0.3464(1)	0.0000	0.5000	0.5807(4)	0.1500(2)
Sr3	0.3369(2)	0.0000	0.0000	0.5807(4)	0.3072(3)
Ca3	0.3369(2)	0.0000	0.0000	0.5807(5)	0.1936(5)
O1	0.4811(3)	0.6459(4)	0.2408(2)	1.4691(2)	1.0000
O2	0.6811(2)	0.1783(3)	0.4520(4)	1.4691(4)	1.0000
O3	0.8423(4)	0.0000	0.0000	1.4691(4)	0.4920(5)
O4	0.6864(4)	0.1814(3)	0.0476(6)	1.4691(3)	0.9834(5)
O5	-0.0039(3)	0.1614(5)	0.3039(6)	1.4691(3)	0.9856(4)
300 K ($a = b = 9.3884(3)$ Å, $c = 7.7118(2)$ Å, $\alpha = \beta = 90°$, $\gamma = 120°$)					
Atom (Site)	x	y	z	B_{iso}	Occupancy
Mn1	0.0000	0.0000	0.1757(4)	0.6823(4)	0.3333(1)
Mn2	0.3333	0.6667	0.0744(2)	0.6823(5)	0.3333(5)
Mn3	0.3333	0.6667	0.3970(3)	0.6823(5)	0.3333(5)
Co1	0.0000	0.0000	0.5000	0.6823(4)	0.1667(3)
Co2	0.3333	0.6667	0.7755(3)	0.6823(5)	0.3333
Sr1	0.0200(1)	0.6878(1)	0.2497(3)	0.5807(3)	0.3602(3)
Ca1	0.0200(1)	0.6878(1)	0.2497(2)	0.5807(4)	0.6408(2)
Sr2	0.3473(3)	0.0000	0.5000	0.5807(5)	0.3337(5)
Ca2	0.3473(4)	0.0000	0.5000	0.5807(3)	0.1669(4)
Sr3	0.3308(2)	0.0000	0.0000	0.5807(5)	0.3072(5)
Ca3	0.3308(3)	0.0000	0.0000	0.5807(4)	0.1936(5)
O1	0.4811(3)	0.6459(4)	0.2408(4)	1.4691(4)	1.0000
O2	0.6819(2)	0.1792(3)	0.4511(3)	1.4691(4)	1.0000
O3	0.8428(3)	0.0000	0.0000	1.4691(4)	0.5000
O4	0.6852(3)	0.1771(4)	0.0469(1)	1.4691(5)	1.0000
O5	-0.0064(2)	0.1600(3)	0.3039(4)	1.4691(5)	1.0000

Table 2: All possible basis vectors for the magnetic moments of Mn(1), Mn(2), Mn(3), and Co(2).

IR	BV	Identical Crystal Sites	$m_{\|\|a}$	$m_{\|\|b}$	$m_{\|\|c}$
Γ_1	Ψ_1	1	0	0	3
		2	0	0	−3
Γ_2	Ψ_2	1	0	0	3
		2	0	0	3
Γ_3	Ψ_3	1	1.5	0	0
		2	−1.5	−1.5	0
	Ψ_4	1	0	1.5	0
		2	0	1.5	0
	Ψ_5	1	0.866	1.732	0
		2	−0.866	0.866	0
	Ψ_6	1	−1.732	−0.866	0
		2	1.732	0.866	0

Γ_i and Ψ_i denote irreducible representations (IRs) and their corresponding basis vectors (BVs), respectively.

Table 3: All possible basis vectors for the magnetic moments of Co(1).

IR	BV	$m_{\|\|a}$	$m_{\|\|b}$	$m_{\|\|c}$
Γ_2	Ψ_1	0	0	6
Γ_3	Ψ_2	0	−1.5	0
	Ψ_3	−1.732	−0.866	0

Γ_i and Ψ_i denote irreducible representations (IRs) and corresponding basis vectors (BVs), respectively.

Table 4: Symmetry-allowed magnetic moment directions for P321 (No. 150) subgroups.

Magnetic Space Group	Multiplicity	Wyckoff Letter	Coordinates
P321 (150.25)	2	d	(1/3, 2/3, z | 0,0,m_z); (2/3, 1/3, −z | 0,0,−m_z)
	2	c	(0,0,z | 0,0,m_z); (0,0,−z | 0,0,−m_z)
	1	b	(0,0,1/2 | 0,0,0)
P32′1 (150.27)	2	c	(0,0,z | 0,0,m_z); (0,0,−z | 0,0,m_z)
	1	b	(0,0,1/2 | 0,0,m_z)

Coordinates are given in fractional crystallographic units with the associated magnetic moment direction (m_z).

found to be 3.24 μ_B, while for Co(2), the moment was 1.14 μ_B. Mn(2) and Mn(3) belong to identical chains, so we introduced a constraint that their magnetic moments are equal. The refined moments for both Mn(2) and Mn(3) were found to be 0.78 μ_B. The refined moment for Mn(1) was determined to be 1.17 μ_B. The relatively high value of the Co(1) moment suggests the presence of an unquenched orbital contribution, which accounts for the strong magnetic anisotropy observed in this system. The high local symmetry of the CoO_6 polyhedron at the Co(1) site likely plays an important role in this crystalline anisotropy, which is absent at the Co(2) site. The bond lengths between magnetic atoms (M–M) and the M–O–M bond angles are provided in Table ST6 for Chain A and Table ST7 for Chain B, respectively. Table ST8 presents the M–O bond lengths at 5 K and 300 K. No significant changes in the M–M bond lengths, M–O–M angles, or M–O bond lengths are observed between the magnetic and paramagnetic regions.

Table 5: Irreducible representations and basis vectors for each Mn-site and Co-site for space group P321 with propagation vector $\mathbf{k} = (0, 0, 0)$.

Atom	IR	BV	Identical Sites	Wyckoff Position	$m_{\|\|a}$	$m_{\|\|b}$	$m_{\|\|c}$
Mn(1)	Γ_3	Ψ_6	1	(0,0,0.1740)	0	0	3
			2	(0,0,0.8259)	0	0	3
Co(1)	Γ_3	Ψ_3	1	(0,0,0.5)	0	0	6
Mn(2)	Γ_3	Ψ_6	1	(0.3333, 0.6667, 0.0710)	0	0	3
			2	(0.6667, 0.3333, 0.9289)	0	0	3
Mn(3)	Γ_3	Ψ_6	1	(0.3333, 0.6667, 0.3948)	0	0	3
			2	(0.6667, 0.3333, 0.6051)	0	0	3
Co(2)	Γ_3	Ψ_6	1	(0.3333, 0.6667, 0.7754)	0	0	3
			2	(0.6667, 0.3333, 0.2245)	0	0	3

Fractional atomic coordinates correspond to positions used in the magnetic structure refinement.

Table 6: M–M distances and M–O–M bond angles in Chain A.

T (K)	Mn(1)–Co(1)	Mn(1)–Mn(1)	Co(1)–O(5)–Mn(1)	Mn(1)–O(3)–Mn(1)
5	2.50	2.68	77.78	84.40
300	2.50	2.71	77.42	85.10

Distances are in Å and bond angles are in degrees.

Table 7: M–M distances and M–O–M bond angles in Chain B.

T (K)	Mn(2)–Co(2)	Mn(3)–Mn(2)	Mn(3)–Co(2)	Co(2)–O(4)–Mn(2)	Mn(2)–O(1)–Mn(3)	Mn(3)–O(2)–Co(2)
5	2.27	2.49	2.93	72.71	79.72	86.68
300	2.30	2.49	2.92	72.20	79.55	86.48

Table 8: All M–O bond distances in SCMCO.

T (K)	Co(1)–O(5)	Mn(1)–O(3)	Mn(1)–O(5)	Co(2)–O(2)	Co(2)–O(4)	Mn(2)–O(4)	Mn(2)–O(1)	Mn(3)–O(2)	Mn(3)–O(1)
5	2.15	2.00	1.82	2.32	2.04	1.78	1.98	1.92	1.91
300	2.15	2.00	1.82	2.32	2.07	1.82	1.97	1.92	1.92

All distances are in Å.

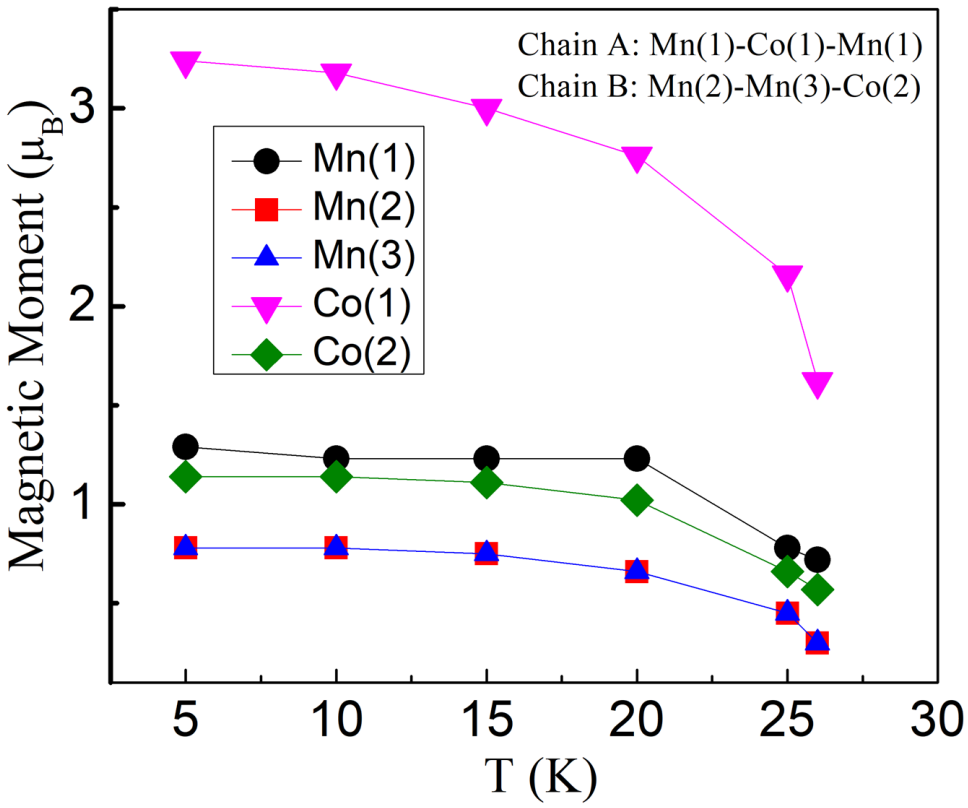

Figure 3: Magnetic moments of individual magnetic atoms as a function of temperature below the ordering temperature.

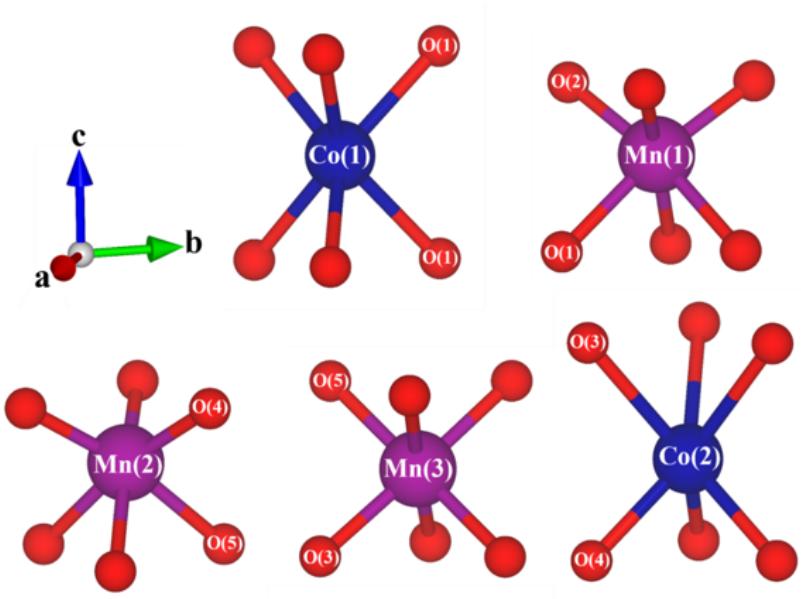

Figure 4: Polyhedral structure of (a) $Co(1)O_6$, (b) $Mn(1)O_6$, (c) $Co(2)O_6$, (d) $Mn(2)O_6$, and (e) $Mn(3)O_6$.

Exchange Interaction: Probability of Electron Hopping from Mn^{4+} to Co^{2+}

At $T = 0$, we consider the initial state as

$$|1\rangle = |\mathrm{Co}^{2+}(\uparrow\downarrow), \mathrm{Mn}^{4+}(\uparrow)\rangle.$$

After a time T, due to electron hopping, the state becomes

$$|2\rangle = |\mathrm{Co}^{2+}(\uparrow), \mathrm{Mn}^{4+}(\uparrow\downarrow)\rangle.$$

We have two linearly independent states:

$$|1\rangle = \begin{pmatrix} 1 \\ 0 \end{pmatrix}, \quad |2\rangle = \begin{pmatrix} 0 \\ 1 \end{pmatrix}.$$

The most general normalized state is a linear combination:

$$|\Psi\rangle = a|1\rangle + b|2\rangle = \begin{pmatrix} a \\ b \end{pmatrix}, \quad |a|^2 + |b|^2 = 1.$$

The Hamiltonian of the system is

$$H = \begin{pmatrix} U & -t \\ -t & U \end{pmatrix},$$

where U is the on-site Coulomb interaction and t is the hopping parameter.

To find the eigenvalues, solve

$$\det(H - EI) = 0 \quad \Rightarrow \quad \det \begin{pmatrix} U - E & -t \\ -t & U - E \end{pmatrix} = 0.$$

This gives

$$E_{1,2} = U \mp t.$$

The corresponding eigenvectors satisfy

$$\begin{pmatrix} U & -t \\ -t & U \end{pmatrix} \begin{pmatrix} a \\ b \end{pmatrix} = E \begin{pmatrix} a \\ b \end{pmatrix} \quad \Rightarrow \quad a = \pm b.$$

Normalized eigenvectors:

$$|\Psi_\pm\rangle = \frac{1}{\sqrt{2}} \begin{pmatrix} 1 \\ \pm 1 \end{pmatrix}, \quad E_{1,2} = U \mp t.$$

The initial state can be expressed as a superposition of eigenstates:

$$|1\rangle = \begin{pmatrix} 1 \\ 0 \end{pmatrix} = \frac{1}{\sqrt{2}} \left(|\Psi_+\rangle + |\Psi_-\rangle \right).$$

The time evolution of the state $|\Psi(T)\rangle$ is governed by the Schrödinger equation:

$$i\hbar \frac{\partial}{\partial T} |\Psi(T)\rangle = H |\Psi(T)\rangle.$$

Using the eigenvalues, the time-evolved state is

$$|\Psi(T)\rangle = \frac{1}{\sqrt{2}} \left[|\Psi_+\rangle e^{-iE_1 T/\hbar} + |\Psi_-\rangle e^{-iE_2 T/\hbar} \right].$$

Substituting $E_1 = U - t$, $E_2 = U + t$ and expanding the eigenvectors:

$$|\Psi(T)\rangle = \frac{1}{2} e^{-iUT/\hbar} \begin{pmatrix} e^{itT/\hbar} + e^{-itT/\hbar} \\ e^{itT/\hbar} - e^{-itT/\hbar} \end{pmatrix}.$$

Using Euler's formula, this simplifies to:

$$|\Psi(T)\rangle = e^{-iUT/\hbar} \begin{pmatrix} \cos(tT/\hbar) \\ \sin(tT/\hbar) \end{pmatrix}.$$

The probability of finding the system in state $|2\rangle$ at time T is

$$P_{1\to 2}(T) = |\langle 2|\Psi(T)\rangle|^2 \propto \sin^2\left(\frac{tT}{\hbar}\right).$$

References

(1) Rodríguez-Carvajal, J. Recent Advances in Magnetic Structure Determination by Neutron Powder Diffraction. *Physica B: Condensed Matter* **1993**, *192*, 55–69.

(2) Wills, A. S. A New Protocol for the Determination of Magnetic Structures Using Simulated Annealing and Representational Analysis (SARAh). *Physica B: Condensed Matter* **2000**, *276-278*, 680–681.

(3) Momma, K.; Izumi, F. VESTA 3 for Three-Dimensional Visualization of Crystal, Volumetric and Morphology Data. *J. Appl. Crystallogr.* **2011**, *44*, 1272–1276.